Available online at www.sciencedirect.com
SCIENCE DIRECT
Journal of the European Ceramic Society 25 (2005) 2235–2240
www.elsevier.com/locate/jeurceramsoc

A microstructure based numerical simulation of microwave sintering of specialized SOFC materials☆

K. Darcovich[a,*], P.S. Whitfield[a], G. Amow[a], K. Shinagawa[b], R.Y. Miyahara[c]

[a] *National Research Council of Canada, Institute for Chemical Process and Environmental Technology, Ottawa, Ont., Canada, K1A 0R6*
[b] *Department of Advanced Materials Science, Faculty of Engineering, Kagawa University, Hayashi-cho 2217-20, Takamatsu 761-0396, Japan*
[c] *Department of Material and Metallurgical Engineering, Polytechnical School, University of São Paulo, São Paulo, SP, C.E.P.: 05508-900, Brazil*

Available online 31 March 2005

Abstract

An on-going project is investigating novel materials such La_2NiO_4 for use as SOFC cathode materials. Owing to their more complex electrochemical properties, these classes of materials have proven to be good electromagnetic susceptors and consequently are being processed with microwave sintering. Finite element code has been developed for simulating the sintering of porous ceramic materials, and is capable of treating local microstructural features derived from the powder properties of the compact. The objective of the project is to develop a microstructure based numerical simulation of heat uptake in a microwave field in order to explore suitable sintering processing conditions and parameter ranges. Specifically, field values of the compact density, particle size distribution and temperature can be traced over time. Since the particle size distribution is a field variable, the simulation should prove to be a useful research tool for microstructure design through powder compact sintering, for novel SOFC materials which have complex responses to microwave energy.

Keywords: Microstructure; Microwave processing; Fuel cells; Numerical simulation

1. Introduction

A solid oxide fuel cell (SOFC) is an electrochemical device that converts the energy of a chemical reaction directly into electrical energy. With a solid electrolyte and high operating temperature, it offers many advantages over conventional power-generating systems in terms of efficiency, reliability, modularity, fuel flexibility, and environmental friendliness.

Developing novel oxide materials with high mixed ionic-electronic conductivity is of considerable interest for numerous applications such as SOFCs, high temperature gas electrolysis, sensors and ceramic membranes. Using mixed conductors as electrode materials for SOCFs and other solid electrolyte cells leads, as a rule, to decreasing polarization losses due to an enlargement of the electrochemical reaction zone.

Planar perovskite-type lanthanum nickelate (La_2NiO_4) has excellent transport and electrocatalytic properties: high electronic conductivity, significant oxygen ion mobility, and noticeable electrochemical and catalytic activity in reactions involving oxygen. Electromagnetic properties include significant dielectric and magnetic losses,[1,2] making it an interesting material for microwave sintering, and thus chosen as the compound to be modelled in this study.

2. Model formulation

2.1. Constitutive model for sintering

A constitutive model for sintering ceramic powders originally developed by Shinagawa and Hirashima[3] is outlined briefly below. Full details of the formulation are given elsewhere.[4]

The principal components of the sintering model are as follows:

☆ NRCC No. 47846. Presented at Electroceramics IX, Cherbourg, France, May 31–June 3, 2004.

* Corresponding author. Tel.: +1 613 993 6848; fax: +1 613 991 2384.
E-mail address: ken.darcovich@nrc-cnrc.gc.ca (K. Darcovich).

0955-2219/$ – see front matter Crown Copyright © 2005 Published by Elsevier Ltd. All rights reserved.
doi:10.1016/j.jeurceramsoc.2005.03.038

An expression from Coble[5] was employed as the basis for sintering deformation under grain boundary diffusion:

$$\dot{\varepsilon} = \frac{47\,\Omega h D_b \sigma}{kTd^3} = \frac{\sigma}{3\eta} \tag{1}$$

where Ω is the atomic volume, h is the width of the grain boundary, D_b is the grain boundary diffusion coefficient, k is Boltzmann's constant, T is the absolute temperature and d is the grain size. From Eq. (1), a number of the parameters can be lumped to give η, the sintering viscosity, which can be considered as a measure of a material's resistance to sintering.

As given by Shinagawa,[6] the constitutive equation for the strain rate $\dot{\varepsilon_{ij}}$, is,

$$\dot{\varepsilon_{ij}} = \frac{1}{2\eta}\,\frac{1}{\rho^{2n-1}}\left\{\sigma'_{ij} + \delta_{ij}\,\frac{2}{9f^2}(\sigma_m + \sigma_s)\right\} \tag{2}$$

Above, ρ is the relative density, σ' is the deviatoric stress, σ_m is the hydrostatic stress, σ_s is the sintering stress, and f and n are empirical parameters.

This strain rate is related to the induced sintering stress,[7] and the flow stress of powder particles during sintering can be solved with a set of discretised equations by the finite element method. The above equations drive deformation mechanisms inducing sample densification.

2.2. Microstructural evolution

The local influence of powder distributions was incorporated into the model with the relation,[8]

$$\frac{\partial \mathcal{F}}{\partial t} + \frac{\partial}{\partial r}\left(\frac{C_G \mathcal{F}}{r^n}\left(\frac{1}{r_c} - \frac{1}{r}\right)\right) = 0 \tag{3}$$

Eq. (3) enables each radius r and its corresponding frequency $\mathcal{F}$ to be solved together in a marching algorithm tracking local particle size distribution evolution.

To account for all pair interactions throughout the entire particle size distribution, the parameter η from Eq. (1) is adjusted according to,

$$\eta_{\mathrm{PSD}} = \left(\frac{\int_{r_S}^{r_L}\int_{r_S}^{r_b} \eta(r_i, r_b)\,\mathcal{F}(r_i)\mathcal{F}(r_b)\,dr_i\,dr_b}{\int_{r_S}^{r_L}\int_{r_S}^{r_b} \mathcal{F}(r_i)\mathcal{F}(r_b)\,dr_i\,dr_b}\right)\left(\frac{C_{N_{\mathrm{AVG}}}}{C_{N_{\mathrm{PSD}}}}\right) \tag{4}$$

Above C_N refers to the coordination number of the powder pack. The particle pair interaction term,

$$\eta(r_i, r_b) = 8K_E\,\frac{r_i^{3.4725}}{r_b^{0.4725}} \tag{5}$$

is a modification of an original derivation by Pan et al.[4,9] Eqs. (4) and (5) are of relevance as the uptake of microwave energy can be input as a function of local powder properties.[10] Data suggest that microwave energy transfer may be a near linear function of the specific surface area of powder.

2.3. Microwave heating

The penetration of microwaves into materials gives rise to a volumetrically distributed heat source. The process combines the propagation and absorption of electromagnetic waves in the ceramic material, heat transport within the body, inducing changes to both macroscopic shape and microstructural morphology.[11]

Energy transfer in microwave-matter interactions can be described by the generalized energy loss equation[12]:

$$P_{\mathrm{MW}} = 2\pi[\epsilon_0\epsilon'_R \tan\delta |E|^2 + \mu_0\mu'_R \tan\phi |H|^2] \tag{6}$$

where ϵ_0 and μ_0 are dielectric permittivity and magnetic permeability of free space, ϵ'_R and μ'_R are the real part of the dielectric permittivity and magnetic permeability of the sample processed, $\tan\delta$ and $\tan\phi$ are the dielectric and magnetic loss factor values, and $|E|$ and $|H|$ are the electric and magnetic field strength inside the sample. Although both E and H fields appear above, most research to date has not considered the magnetic contribution. Dielectric and magnetic loss can lead to thermal runaway and uneven heating in materials with low thermal conductivity.

To obtain the temperature distribution in the sample at each time step, the heat transport equation must be solved with the appropriate boundary conditions. It incorporates the conversion of microwave energy to thermal energy, as well as thermal losses to the environment. For the 2D case, this equation is:

$$\frac{\rho c}{k_T}\,\frac{\partial T}{\partial t} = \frac{\partial^2 T}{\partial x^2} + \frac{\partial^2 T}{\partial y^2} + P_{\mathrm{MW}}(x, y, t) - Q_R - Q_C \tag{7}$$

where c is the heat capacity per unit volume, ρ the density, T the temperature, t the time, k the thermal conductivity, P_{MW} the microwave power, Q_R the radiation heat transfer and Q_C the convection heat transfer.

The electric field is assumed to decay (at a position x) within the sample according to:

$$E = E_0 \exp\left(\frac{-x}{d}\right) \tag{8}$$

where d is the skin depth and E_0 is the electric field in the unloaded cavity, which is proportional to the microwave power temporal profile.[13] For a multimode microwave source, the magnetic field properties can be considered as equivalent to the electric field.[14] The skin depth is related to the frequency of the microwave source and to the loss tangent through:

$$d(T, \rho, f) = \frac{0.0675}{f\sqrt{\epsilon'_R}\sqrt{\sqrt{1 + \tan^2\delta} - 1}} \tag{9}$$

The Q_R and Q_C terms are detailed in.[15]

3. Experimental

The particle size distribution of a La_2NiO_4 sample was used as a basis for the powder properties of the structures. The measured particle size distribution is shown at the $t = 0$ step in Fig. 4. The powder had a specific surface area of 4.149 m^2/g, determined by a spherical grain assumption integration. Powder size distributions were determined using a Horiba model LA-920 Particle Size Analyzer, which is a laser diffraction device.

4. Material parameters

For preliminary code validation, data from the literature were found for alumina thermal properties across the relevant temperature range.[16,17]. Other sintering parameters for alumina and and all the data for silicon carbide were found in.[18]

For La_2NiO_4 an extensive set of material properties over a broad temperature range was required. In some cases, only partial data was found, so estimates were made based on basic trends observed in the K_2NiF_4 structural family, and comparative tendencies between nickel and other metallic elements. For cases where parameters were constructed from partial sources, sample values are given below for temperatures of 300, 800 and 1300 K.

Thermal conductivity data have been published by Pillai and George,[19] and heat capacity data from Castro and Burriel were used,[20] (364.67, 488.47, 564.51; [J/kg K]). Radiative heat transfer parameters were published by Tsaneva et al.[21] (0.930, 0.913, 0.767). Dielectric properties (ϵ: 12.74, 14.93, 15.99), ($\tan\delta$: 5.953×10^{-6}, 1.814×10^{-5}, 2.013×10^{-5}) were taken from[1,22,23], and magnetic properties (μ: 7.744×10^5, 8.535×10^3, 1.699×10^2), ($\tan\phi$: 3.565, 0.138, 0.081) were given in.[2,24] Surface free energy data (2.01, 1.91, 1.81; [J/m^2]) were estimated based on papers from Aldén et al.[25] and Read et al.[26] The D_b function for sintering ($2.467 \times 10^{-9} \exp(-6400.0/T)$ [m^3/s]) was obtained from Kilner and Shaw.[27]

A density value of 7070 kg/m^3 was used, based on a crystallographic calculation. Also from this calculation, a molecular volume of 9.4106×10^{-29} m^3 was determined.

5. Simulation conditions

The simulation modelled microwave heating with a 2.45 GHz multimode source at a power output of 700 W in a cavity volume of 10^{-3} m^3, approximating a unit in our laboratories. The samples considered were flat discs, 13 mm in diameter and 4 mm in height, treated in two dimensions with a central vertical symmetry plane. The rectangular finite element grid had 34 horizontal and 10 vertical elements. Boundary conditions were symmetry conditions on the left side, the top and right sides were exposed to microwaves and to convective gas at 300 K, and the bottom surface was considered insulated. The cavity surface temperature was set to 353 K. The electrical field strength in the cavity was calculated according to Metaxas and Meredith.[28] The convective heat transfer coefficient was set to 1.5 W/m^2 K. Initial fractional densities in the structures were set to 0.65, and the initial temperature was set to 300 K. Based on previous sintering simulation work, the sintering time step was set to 60 s. The simulation then consisted of setting the microwave power on, and tracing the heating and heat transfer in the structure, which drove the densification and grain coarsening mechanisms, over a period of 60 virtual minutes.

6. Results and discussion

Some code verification work was performed to find a suitable time step for the heat uptake from the microwaves. Since the calculated changes are rate driven, it was necessary to arrive at a fine enough time step to ensure numerical stability. For the microwave heating, a time step of 0.1 s was nested into the 60 s sintering time step and gave time-temperature results which closely matched heating curves for both alumina and silicon carbide shown by Chatterjee et al.[18]

Next, properties for La_2NiO_4 were input to the simulation. Fig. 1 shows the resulting heating curve. The temperature from the top left element of the structure was used here. Since the samples considered were quite small, there was minimal (less than 2 K) temperature variation in the structure. A further reason for this is that with thin samples, the microwave penetration depth is sufficient to heat the entire volume uniformly. The shape of the curve roughly corresponds to the temperature functionality of the loss coefficients. The final temperature reached after one hour was 1354 K, very similar to an estimate of 1100 °C observed experimentally in our laboratories. Literature data from Panneerselvam and Rao[29] shows a 300 W microwave bringing the chemically similar, but less electromagnetically responsive $LaNiO_3$ together with an SiC susceptor to 1073 K in 50 min, compared to 1151 K in the present study. The lower curve in Fig. 1 shows output where the magnetic contribution to heating was set to zero. The temperatures attained are very much lower, and in view of some experimentally observed results, it is clear that the magnetic loss is an essential component for modelling the microwave heating of lanthanum oxides.

The time-temperature profile output in Fig. 1 was used as a basis to compare microwave sintering to conventional sintering. A simulation was run using these temperatures as a boundary condition for the top and right surfaces of the disc, and allowing heat to be conducted into interior regions. A number of studies have shown that the activation energy for diffusion can be significantly decreased in a microwave field[30,31], so to demonstrate this effect, the diffusion activation energy for the conventional heat case

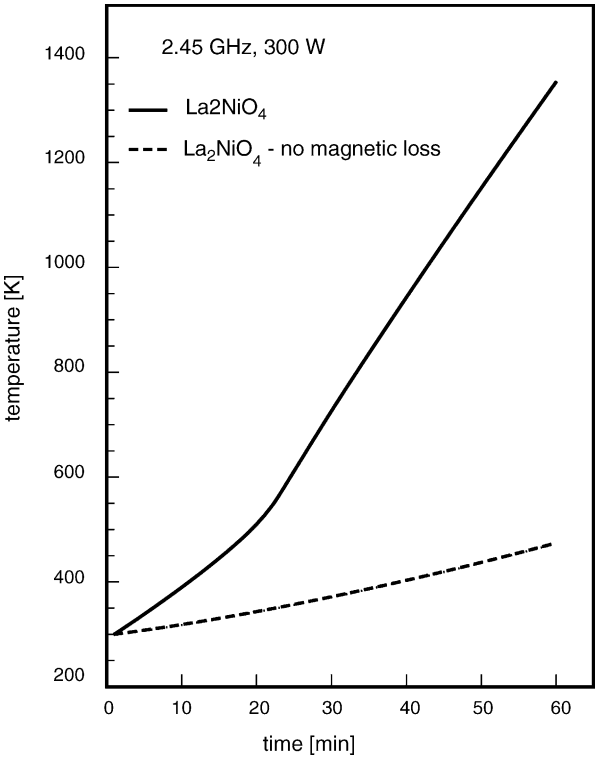

Fig. 1. Heating curves for La_2NiO_4 microwaved for 1 h.

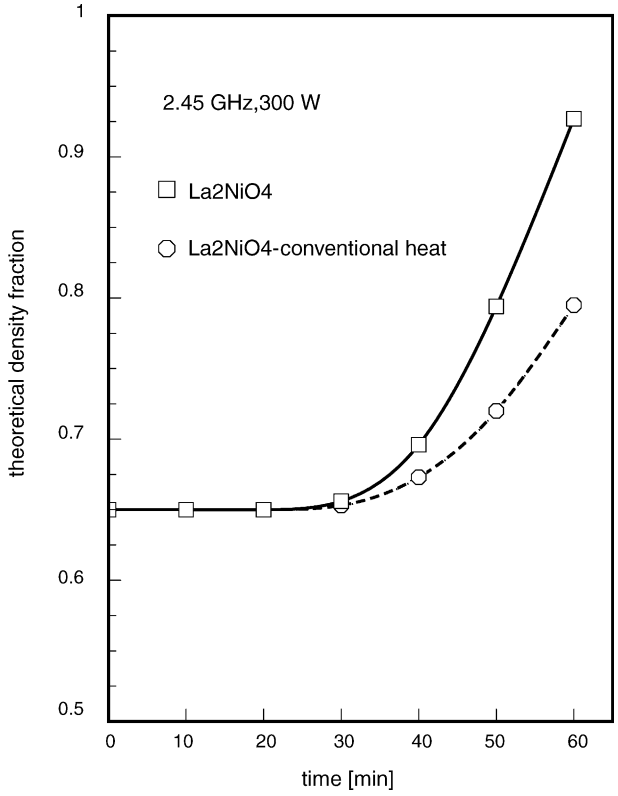

Fig. 2. Densification curves for microwave and conventional sintering cases.

was increased by 30%. In view of the above claims where the activation energy was stated to have been reduced by almost an order of magnitude, other studies have specifically investigated the mechanisms behind enhanced sinterability in microwave fields. These studies suggest that much of what is reported as an enhancement can be attributed to imprecise temperature measurements, and suggest that the actual benefit of the microwave field may be worth about 50 K.[32,33]

Fig. 2 shows the densification rate of a microwaved sample, and one heated conventionally. The lower diffusion rates produce the lower final density for the conventional case. The comparison in Fig. 2 is not really practical as conventional ovens cannot be controlled well enough to follow the heating curve so precisely. Fig. 3 shows the effect of the densification on the profiles of the structures after one hour of sintering. The microwaved sample has a smaller final sintered size compared to the conventionally heated sample, corresponding to its higher density. Of further interest here is the calculation in the left hand sample showing the result when the specific surface area factor for heat uptake is not considered. As the sintering proceeds, grain growth occurs, thereby reducing the heat uptake. Without this factor, a slightly higher final temperature is reached as well as a slightly higher density of 0.944, compared to 0.927. For the sample on the right side, the magnetic loss contribution was not included, and temperatures producing any degree of densification were never reached.

Grain coarsening was also a feature of the simulation, with particle size distributions being traced via Eq. (3). Fig. 4 shows the initial and final particle size distributions for the top left element in the structure. Both microwaved and conventionally heated samples are shown. For the non-microwaved sample, the lower densification rates produce correspondingly less grain growth. Larger grain sizes are less desirable for SOFC materials, but can be controlled to some extent by the initial particle size distribution in the green body.

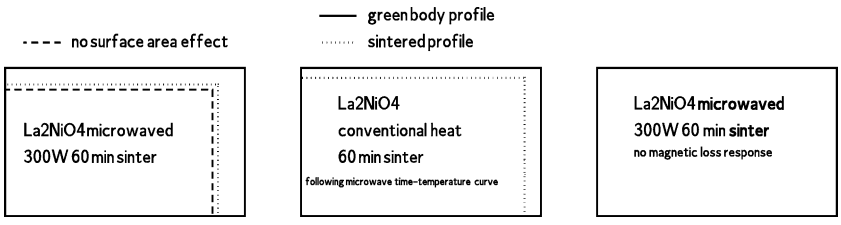

Fig. 3. Shrinkage of discs under various processing conditions.

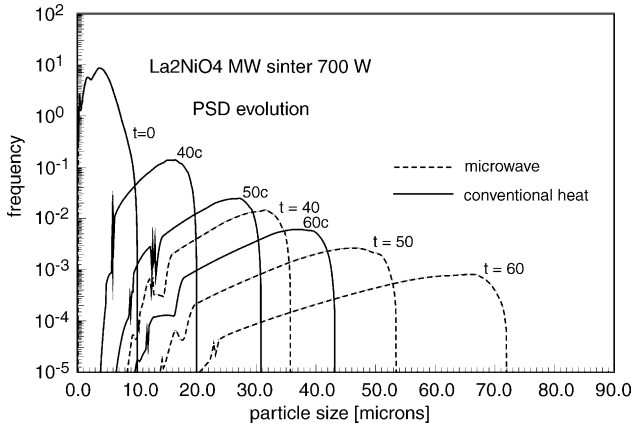

Fig. 4. Particle size distribution evolution during sintering.

7. Conclusions

The discussion above has demonstrated that a fairly complete simulation has been assembled. The model takes into consideration the sintering of a macroscopic porous ceramic body, heated by microwave energy with both dielectric and magnetic responses, which traces its the microstructural evolution. The heat uptake is treated in a transport equation over the body which conducts, convects and radiates heat.

Preliminary calculations have been made using the model compound La_2NiO_4 which has a complex microwave behaviour. The output is qualitatively sound and in the absence of very precise material parameters, gives quantitative output in quite correct ranges of measured data.

This simulation is thus poised to serve as a very useful research tool for sintering operations connected to SOFC electrode development. Since the simulation handles the particle size distribution as a local field variable, microstructure control can be achieved by fine tuning power inputs as well as judiciously preparing powders with distribution qualities amenable to good sintered properties. Further uses are envisioned for defining processing tolerances in powder compact properties to avoid defects, cracks and/or thermal runaway.

References

1. Iguchi, E., Satoh, H., Nakatsugawa, H. and Munakata, F., Correlation between hopping conduction and transferred exchange interaction in $La_2NiO_{4+\delta}$ below 300 K. *Physica B*, 1999, **270**(3–4), 332–340.
2. Giannakopoulou, T., Kompotiatis, L., Kontogeorgakos, A. and Kordas, G., Microwave behavior of ferrites prepared via sol-gel method. *J. Magn. Magn. Mater.*, 2002, **246**(3), 360–365.
3. Shinagawa, K. and Hirashima, Y., A constitutive model for sintering of ceramic powder compacts with internal structure due to granules. *JSME Int. J. Ser. A*, 1999, **42**(1), 17–24.
4. Darcovich, K., Béra, L. and Shinagawa, K., Particle size distribution effects in an FEM model of sintering porous ceramics. *Mater. Sci. Eng.: A*, 2003, **341**, 247–255.
5. Coble, RL., A model for boundary diffusion controlled creep in polycrystalline materials. *J. Appl. Phys.*, 1963, **34**(6), 1679–1682.
6. Shinagawa, K., Finite element simulation of sintering process. *JSME Int. J. Ser. A*, 1996, **39**(4), 565–572.
7. Shinagawa, K., Micromechanical modeling of viscous sintering and a constitutive equation with sintering stress. *Comp. Mater. Sci.*, 1999, **13**, 276.
8. Sivakumar, S., Pradip, Kapur, P.C. and Malghan, S.G., A size interval-by-size interval marching algorithm for modelling grain growth in the intermediate stage of sintering. *Colloids Surf. A: Physiochem. Eng. Aspects*, 1998, **133**, 173–182.
9. Pan, J., Le, H., Kuchernko, S. and Yeomans, J.A.., A model for the sintering of spherical particles of different sizes by solid state diffusion. *Acta Mater.*, 1998, **46**(13), 4671–4690.
10. Leparoux, S., Vaucher, S., and Beffort, O., Influence of SiC-Particle Size on Microwave Sintering of Metal Matrix Composites, 5. Werkstofftechnisches Kolloquium, Chemnitz, 24–25 Oct. 2002, 11, 13–19.
11. Birnboim, A.,and Carmel, Y., Simulation of microwave sintering of ceramic bodies with complex geometry. *J. Am. Ceram. Soc.*, 1999, **82**(11), 3024–3030.
12. Roy, R., Peelamedu, R., Grimes, C., Cheng, J. and Agrawal, D., Major phase transformations and magnetic property changes caused by electromagnetic fields at microwave frequencies. *J. Mater. Res.*, 2002, **17**(12), 3008–3011.
13. Birman, A., Levush, B., Carmel, Y., Gershon, D., Dadon, D.,and Martin, L.P., Modeling of multifrequency microwave sintering of ZnO ceramic. *Ceramic Transactions*, 1995, **59**, 305–312.
14. Cheng, J., Roy, R. and Agrawal, D., Experimental proof of major role of magnetic field losses in microwave heating of metal and metallic composites. *J. Mater. Sci. Lett.*, 2001, **20**, 1561–1563.
15. Tucker, J., Iskander, M.F. and Huang, Z., Calculation of heating patterns in microwave sintering using a 3-D finite difference code. *Mater. Res. Soc. Symp. Proc.*, 1994, **347**, 353–362.
16. Miyayama, M., Koumoto, K., Yanagida, H. Engineering properties of single oxides. In: Schneider Jr S.J., editor. *Engineered Materials Handbook*, **vol. 4**. ASM International; 1991. 748–757.
17. Nishijima T, Kawada T and Ishihata A., Thermal Conductivity of Sintered UO_2 and Al_2O_3 at High Temperatures. *J. Am. Cer. Soc.*, 1965, **48**, 31–34.
18. Chatterjee, A., Basak, T., Ayappa, K.G., Analysis of microwave sintering of ceramics. *AIChE J.*, 1998, **44**(10), 2302–2311.
19. Pillai, C.G.S. and George, A.M., Thermal conductivity of La_2CuO_4, La_2NiO_4 and Nd_2CuO_4 in the semiconducting and metallic phases. *Int. J. Thermophys.*, 1986, **7**(5), 1091–1100.
20. Castro, M. and Burriel, R., Heat capacity study of La_2NiO_4 and Pr_2NiO_4. *Thermochimica. Acta*, 1995, **269/270**, 537–552.
21. Tsaneva, V.N., Tsanev, V.I., Tarte, E.J., Barber, Z.H., Kahlmann, F. and Gibson, G., *et al.* Study of the radiative heating for deposition of high-T_c superconducting thin films. *Vacuum*, 2000, **58**(2–3), 454–463.
22. Liu, X.Q., Chen, X.M. and Xiao, Y., Preparation and characterization of $LaSrAlO_4$ microwave dielectric ceramics. *Mater. Sci. Eng.: B*, 2003, **103**, 276–280.
23. Fuschillo, N., Lalevic, B. and Leung, B., Electrical conduction and dielectric breakdown in crystalline NiO and NiO(Li) films. *J. Appl. Phys.*, 1975, **46**(1), 310–316.
24. Schartman, R.R. and Honig, J.M., Magnetic susceptibility investigations of the $La_2NiO_{4+\delta}$ system. *Mat. Res. Bull.*, 1989, **24**, 671–679.
25. Aldén, M., Skriver, H.L., Mirbt, S. and Johansson, B., Calculated surface-energy anomaly in the 3d metals. *Phys. Rev. Lett.*, 1992, **69**(15), 2296–2298.
26. Read, M.S.D., Islam, M.S., Watson, G.W. and Hancock, F.E., Defect Chemistry and Surface Properties of $LaCoO_3$. *J. Mater. Chem.*, 2000, **10**, 2298–2305.
27. Kilner, J.A. and Shaw, C.K.M., Mass transport in $La_2Ni_{1-x}Co_xO_{4+\delta}$ oxides with the K_2NiF_4 structure. *Solid State Ionics*, 2002, **154–155**, 523–527.
28. Metaxas, A.C., Meredith, R.J. Industrial Microwave Heating. London: Peregrinus; 1983.

29. Panneerselvam, M. and Rao, J.K., Microwave preparation and sintering of industrially important perovskite oxides: $LaMO_3$ (M = Cr, Co, Ni). *J. Mater. Chem.*, 2003, **13**, 596–601.
30. Dadon, D., Martin, D.L., Rosen, M., Birman, A., Gershon, D. and Calame, J.P., *et al*. Temperature and porosity gradients developed during nonisothermal microwave processing of Zinc oxide. *J. Mater. Synth. Proc.*, 1996, **4**(2), 95–103.
31. Brosnan, K.H., Messing, G.L. and Agrawal, D.K., Microwave sintering of alumina at 2.45 GHz. *J. Am. Cer. Soc.*, 2003, **86**(8), 1307–1312.
32. Boch, P. and Lequeux, N., Do microwaves increase the sinterability of ceramics? *Solid State Ionics*, 1997, **101–103**, 1229–1233.
33. Aguilar, J. and Valdez, Z., Effecto catalítico de las microondas en la producción de $MgAl_2O_4$. *Ingenierías*, 2002, **5**(15), 13–18.